A novel animal model of Epstein-Barr virus–associated hemophagocytic lymphohistiocytosis in humanized mice

Kei Sato,[1,2] Naoko Misawa,[1] Chuanyi Nie,[1] Yorifumi Satou,[3] Dai Iwakiri,[4] Masao Matsuoka,[3] Rei Takahashi,[5,6] Kiyotaka Kuzushima,[7] Mamoru Ito,[8] Kenzo Takada,[4] and Yoshio Koyanagi[1]

[1]Laboratory of Virus Pathogenesis, [2]Center for Emerging Virus Research, and [3]Laboratory of Viral Control, Institute for Virus Research, Kyoto University, Kyoto, Japan; [4]Department of Tumor Virology, Institute for Genetic Medicine, Hokkaido University, Sapporo, Japan; [5]Pathology and Tumor Biology, Graduate School of Medicine, Kyoto University, Kyoto, Japan; [6]Doshisha Women's College of Liberal Arts, Kyotanabe, Japan; [7]Laboratory of Viral Oncology, Aichi Cancer Center, Nagoya, Japan; and [8]Central Institute for Experimental Animals, Kawasaki, Japan

EBV-associated hemophagocytic lymphohistiocytosis (EBV-HLH) is a rare yet devastating disorder caused by EBV infection in humans. However, the mechanism of this disease has yet to be elucidated because of a lack of appropriate animal models. Here, we used a human CD34$^+$ cell-transplanted humanized mouse model and reproduced pathologic conditions resembling EBV-HLH in humans. By 10 weeks postinfection, two-thirds of the infected mice died after exhibiting high and persistent viremia, leukocytosis, IFN-γ cytokinenemia, normocytic anemia, and thrombocytopenia. EBV-infected mice also showed systemic organ infiltration by activated CD8$^+$ T cells and prominent hemophagocytosis in BM, spleen, and liver. Notably, the level of EBV load in plasma correlated directly with both the activation frequency of CD8$^+$ T cells and the level of IFN-γ in plasma. Moreover, high levels of EBV-encoded small RNA1 were detected in plasma of infected mice, reflecting what has been observed in patients. These findings suggest that our EBV infection model mirrors virologic, hematologic, and immunopathologic aspects of EBV-HLH. Furthermore, in contrast to CD8$^+$ T cells, we found a significant decrease of natural killer cells, myeloid dendritic cells, and plasmacytoid dendritic cells in the spleens of infected mice, suggesting that the collapse of balanced immunity associates with the progression of EBV-HLH pathogenesis. (*Blood*. 2011;117(21):5663-5673)

Introduction

EBV is a human-specific double-stranded DNA virus that belongs to *Gammaherpesvirinae*.[1] EBV is one of the most commonly found viruses in humans, infecting 90% of adults worldwide.[1] Primary infection of EBV can manifest into infectious mononucleosis, which is a condition characterized by lymphadenopathy and the appearance of atypical CD8$^+$ T cells in the peripheral blood (PB).[1,2] Infectious mononucleosis is usually a self-limiting and nonlife-threatening condition that does not require specific treatment.[1,2] However, EBV infection can also result in serious conditions such as Burkitt lymphoma, Hodgkin lymphoma, and other B-cell lymphomas.[1,2] Among the disorders induced by EBV infection, hemophagocytic lymphohistiocytosis (HLH) is one of the most devastating.

HLH is an immunopathologic entity characterized by an uncontrolled activation of the immune system.[3-5] In patients with HLH, persistent activation of CD8$^+$ T cells and innate immune cells lead to the overproduction of proinflammatory cytokines such as IFN-γ and TNF-α.[3] The elevated concentration of the proinflammatory cytokines drives further proliferation and activation of CD8$^+$ T cells and macrophages/histiocytes.[3] Activated macrophages/histiocytes engulf blood cells, a process called hemophagocytosis, and cause erythrocytopenia and thrombocytopenia.[3-5] Activated CD8$^+$ T cells invade organs systemically, causing hepatomegaly, splenomegaly, inflammation, and organ failure.[3-6]

The mortality rate of HLH can be as high as 50% even with treatment.[6] Currently, there are no specific therapies against HLH[3,6] and options for HLH therapy are limited to supportive care and combined immunosuppressive regimens. However, the latter treatment can lead to complications such as life-threatening infections.

HLH can be categorized into 2 types, congenital HLH and acquired HLH. Congenital HLH is associated with predisposing genetic mutations, whereas acquired HLH is not. In one example of congenital HLH, mutations in *PRF1* (encodes Perforin) cause impaired cytolytic granule formation, which leads to the development of HLH.[7,8] X-linked lymphoproliferative syndrome (XLP) is also one of the congenital HLHs and is followed by primary EBV infection. Genetic mutations in *SAP/SH2D1A* (encodes SLAM-associated protein [SAP])[9] or *XIAP/BIRC4* (encodes X-linked inhibitor-of-apoptosis [XIAP])[10] are responsible for XLP. Dysfunction of SAP can cause multiple immune impairments, including inefficient effector function of HLA-restricted EBV-specific CTLs,[11] whereas dysfunction of XIAP leads to the deregulation of lymphocyte homeostasis.[10]

To reproduce the pathogenesis of congenital HLH, representative mouse models have been reported.[12,13] For instance, *Sap* (encodes Sap, the ortholog of *SAP/SH2D1A* in human) knockout mice,[13] and *Prf* (encodes Perforin) knockout mice[12] exhibit XLP-like disorders after infection with lymphocytic choriomeningitis virus (LCMV). These LCMV-infected knockout mice showed

Submitted September 10, 2010; accepted March 16, 2011. Prepublished as *Blood* First Edition paper, April 5, 2011; DOI 10.1182/blood-2010-09-305979.

The online version of this article contains a data supplement.

The publication costs of this article were defrayed in part by page charge payment. Therefore, and solely to indicate this fact, this article is hereby marked "advertisement" in accordance with 18 USC section 1734.

persistent activation of $CD8^+$ T cells, elevated proinflammatory cytokines, including IFN-γ and TNF-α in plasma, and high rates of mortality.[12,13] LCMV-infected *Prf* knockout mice also displayed hepatosplenomegaly, anemia, and activation of phagocytes.[12]

In contrast to congenital HLH, acquired HLH is not associated with any genetic defects but can be triggered by malignancies and/or infections.[3-5] As an animal model of acquired HLH, it has been recently reported that a conventional mouse infected with *Salmonella enterica* serotype typhimurium exhibits HLH-like disorders.[14] However, bacterial infection-associated HLH only represents a small fraction of infection-associated HLH in humans.[7] EBV is responsible for up to 70% of infection-associated HLH in humans.[15] Therefore, it is important to reproduce the pathogenesis of EBV-HLH in experimental models with human immunity.

To reproduce human immunity and the diseases caused by human-specific pathogens such as HIV-1 and EBV in animals, humanized mouse models have been generated by transplanting human $CD34^+$ hematopoietic stem cells (hHSCs) into lines of immunodeficient mice.[16-21] Previous studies on EBV infection in humanized mouse models were successful in reproducing EBV-associated B-cell malignancies[16,21] and/or human immune responses against EBV antigens.[17,18,20,21] However, none so far has shown EBV-HLH in humanized mice.

In this study, we demonstrate a humanized mouse model of EBV-HLH. The infection of newborn immunodeficient mice xenotransplanted with hHSCs (NOG-hCD34 mice) with EBV resulted in cardinal features of HLH, including hemophagocytosis, erythrocytopenia, thrombocytopenia, hypercytokinemia, $CD8^+$ T-cell activation/proliferation and organ infiltration, and histiocyte proliferation. Moreover, the disease severity, IFN-γ production, and $CD8^+$ T-cell activation correlated with EBV DNA production.

Methods

Generation of NOG-hCD34 mice

NOD/ShiJic-*scid* $\gamma_c^{-/-}$ (NOG) mice[22] were obtained from the Central Institute for Experimental Animals. The mice were maintained under specific pathogen-free conditions and were handled in accordance with the Regulation on Animal Experimentation at Kyoto University. Fresh human cord blood was obtained with the parent's written informed consent from healthy full-term newborns, and $CD34^+$ hHSCs were purified and transplanted into NOG mice as previously described.[23-25] HLA class I typing was performed by an HLA laboratory, and the results are summarized in supplemental Table 1 (available on the *Blood* Web site; see the Supplemental Materials link at the top of the online article). Body weights of mice were routinely measured, and the mice were anesthetized and killed when the weights became $< 75\%$ of their maximum weight or at 10 weeks postinfection (wpi).

Virus preparation and infection

EBV (strain Akata) was prepared and titrated as described previously.[26] One thousand TD_{50} of EBV solution or RPMI (for mock-infection) was intravenously inoculated into NOG-hCD34 mice between 13 and 16 weeks of age.

PB collection and isolation of nucleated cells from organs

PB was collected weekly as described previously.[23-25] Mononuclear cells (MNCs) in PB (PBMCs), spleen, BM, liver, lung, kidney, and ascitic lavage fluid were collected as previously described.[23-25] Human leukocytes were further purified from the MNCs by the use of Ficoll-Paque (Pharmacia), and murine leukocytes were purified from the MNCs by the use of lympholyte-M (Cedarlane Ltd).

Hemocytometry

The levels of leukocytes, erythrocytes, platelets, hematocrit, and hemoglobin in PB and the levels of mean cell volume (MCV), mean cell hemoglobin (MCH), and mean cell hemoglobin concentration (MCHC) in erythrocytes were measured by Celltac α MEK-6450 (Nihon Kohden Co).

Flow cytometry and cell sorting

Flow cytometry was performed with FACSCalibur and FACSCanto (BD Biosciences) as previously described.[23-25,27,28] Anti–human CD45RA-biotin, CD45RO-APC, HLA-DR-PE, Ki67-PE (BD Biosciences), CD11c-APC, CD56-FITC, FOXP3-PE (BioLegend), CD3-PE, CD4-PE, CD8-FITC, CD8-APC, CD19-FITC (Dakocytomation), CD45-biotin (eBiosciences), CD38-biotin, CD303-FITC (Miltenyi Biotec), and anti–murine CD45-PE (ImmunoTech) antibodies were used. For detection of biotinylated antibodies, streptavidin-conjugated PerCP (BD Biosciences) was used. Human $CD4^+$, $CD8^+$, $CD19^+$, and murine $CD45^+$ cells were sorted from splenic MNCs by FACSAria (BD Biosciences). The purity of each population was $> 95\%$.

Tetramer staining

PE-conjugated HLA-A*2402 tetramers mounted with 5 different EBV antigen peptides (derived from BRLF1, BMLF1, LMP2, EBNA3A, and EBNA3B) and PE-conjugated HLA-A*2402 tetramers mounted with HIV-1 Gag antigen peptides were purchased from medical and biologic laboratories, and the staining was performed according to manufacturer's protocol.

Histologic analyses

Preparation of frozen organ sections was conducted as previously described.[29] H&E staining, Berlin blue staining, Giemsa staining, and nonspecific esterase (NSE) staining were performed by conventional methods, respectively.

Immunostaining and in situ hybridization

Immunostaining was performed as previously described.[23] Rabbit anti–human CD8 (Lab Vision), mouse anti–human CD68 (BD Biosciences), anti–human CD20 (Dakocytomation), anti-ZEBRA (Santa Cruz Biotechnology), and anti-gp110 (Cl.50-1) monoclonal antibodies were used as primary antibodies, and appropriate secondary antibodies were used for detection. In situ hybridization for EBV-encoded small RNAs (EBERs) was performed by Kyodo Byori Inc.

PCR and RT-PCR

DNA was extracted from whole PB (30 μL), plasma (30 μL), human MNCs, and murine MNCs with the QIAamp DNA Micro kit (QIAGEN) or DNeasy Blood and Tissue kit (QIAGEN). EBV genomic DNA was quantified by real-time PCR as previously described,[30] and EBV quantified viral DNA control (Advanced Biotechnologies) was used as the standard. The cell number was also quantified by real-time PCR with the use of TaqMan β-actin control reagents (Applied Biosystems), and quantified PBMC genomic DNA was used as the standard. RNA was extracted by the use of RNeasy Mini kit (QIAGEN). Primers used for RT-PCR are listed in supplemental Table 2.

Quantification of cytokines and EBV-encoded small RNA1 in plasma

Quantification of IFN-γ and TNF-α in 10 μL of plasma was performed by the use of cytometric bead array system according to the manufacture's protocol (BD Biosciences). Quantification of IFN-β was performed by the use of a human IFN-β ELISA kit (PBL Biomedical Laboratories).

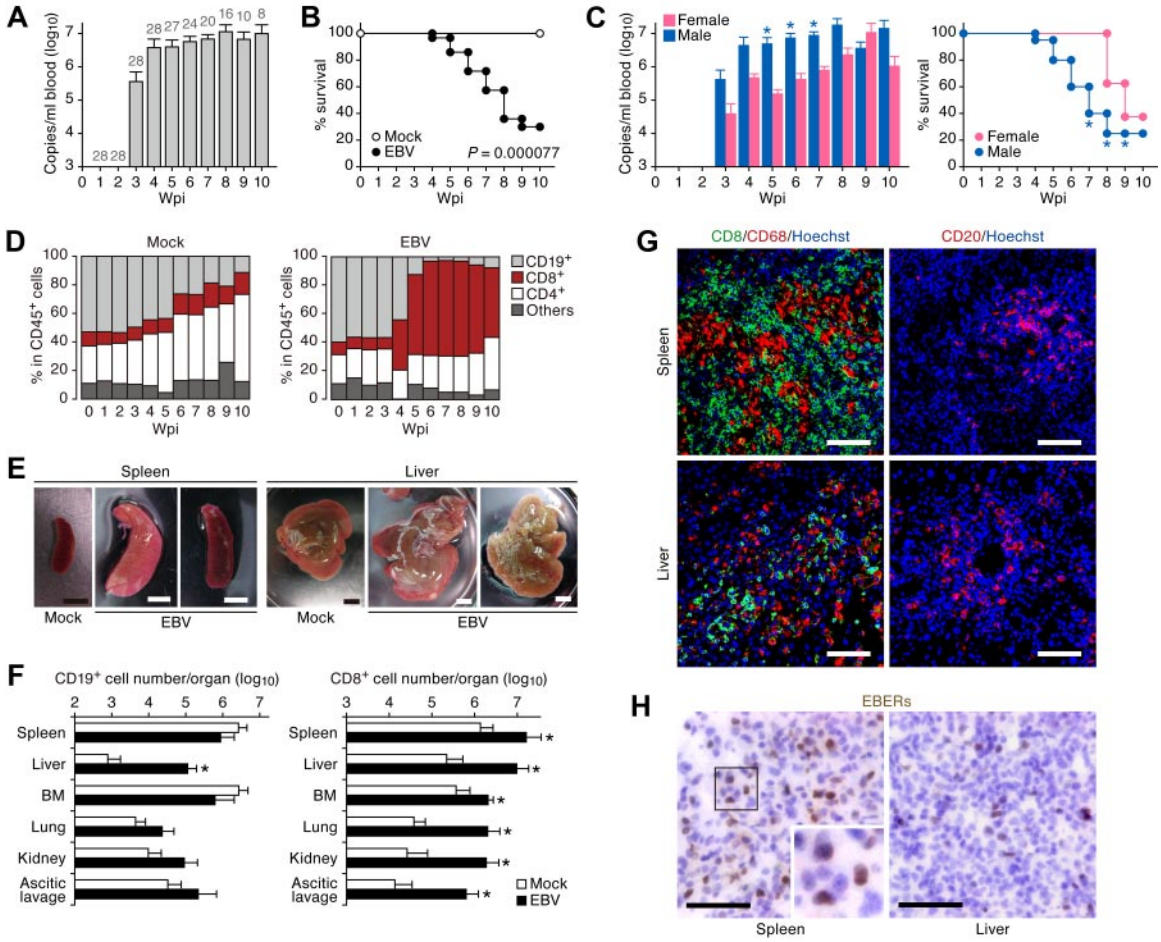

Figure 1. Fatal outcome of EBV-infected NOG-hCD34 mice with persistent viremia, expansion of CD8$^+$ T cells, and hepatosplenomegaly in the absence of B-cell proliferative disorders. (A) Quantification of EBV DNA in the PB of EBV-infected mice. Number at the top of each gray bar represents the number of analyzed EBV-infected mice at each time point. (B) Survival curve. Kaplan-Meier survival curve of mock-infected mice (n = 15) and EBV-infected mice (n = 28) is shown. Statistical significance in the survival rate ($P = .000077$) between mock-infected mice and EBV-infected mice was determined by log-rank test. (C) The difference in the viremia and the survival rate between male and female recipient mice. (Left) The level of EBV DNA in the PB of EBV-infected male mice (n = 20) and EBV-infected female mice (n = 8). Asterisks represent statistic significance ($P < .05$ by Welch t test) versus the value obtained from EBV-infected female mice. (Right) Survival curve. Kaplan-Meier survival curve of EBV-infected male mice (n = 20) and EBV-infected female mice (n = 8) is shown. Statistical significances in the survival rate between EBV-infected male mice and EBV-infected female mice until the indicated wpi were determined by log-rank test. (D) Longitudinal analysis on human PBMC composition. PB was routinely collected from mock-infected mice (n = 5) and EBV-infected mice (n = 12) and was analyzed by flow cytometry. Results are presented as the average percentages in human CD45$^+$ leukocytes. (E) Hepatosplenomegaly in EBV-infected mice. Representatives of spleens and livers of a mock-infected and 2 EBV-infected mice are shown. Scale bars in panel E represent 5 mm. (F) Human MNC numbers in multiple organs. The cell numbers of CD19$^+$ B cells (left) and CD8$^+$ T cells (right) in spleen, liver, BM, lung, kidney, and ascitic lavage fluid of mock-infected mice (n = 4) and EBV-infected mice (n = 7) are shown. Asterisks represent statistic significance ($P < .05$ by Welch t test) versus the value obtained from the mock-infected mice. (G) Immunostaining for CD8, CD68, and CD20. Representatives of spleen (top) and liver (bottom) of EBV-infected mice, respectively, are shown. CD8$^+$ cells (left) and CD20$^+$ cells (right) are shown in green, CD68$^+$ cells (left) are shown in red, and nuclei were shown in blue by staining with Hoechst. (H) In situ hybridization for EBERs. Representatives of spleen (left) and liver (right) of EBV-infected mice were shown. EBERs were shown in brown. Areas enclosed with squares are enlarged in bottom right of the panel. Scale bars in panels G and H represent 50 μm.

EBV-encoded small RNA1 (EBER1) in plasma was quantified as previously described.[31]

Statistic analyses

Statistic differences were determined by paired t test, Student t test, or Welch t test, and $P < .05$ was considered statistically significant. The log-rank test was adopted to determine the statistical significance of survival rates (Figure 1B-C). To determine the statistically significant correlation, the Spearman rank correlation coefficient (r_s) was adopted (Figure 5E-G). Data are presented as mean ± SEM.

Ethics statement

All protocols involving human subjects were reviewed and approved by the Kyoto University Institutional Review Board. Informed written consents from the human subjects were obtained in this study in accordance with the Declaration of Helsinki.

Results

High mortality from EBV infection with systemic organ infiltration by CD8$^+$ T cells in the absence of EBV-associated B-cell proliferative disorders

Newborn NOG mice were transplanted with hHSCs via intrahepatic injection to generate NOG-hCD34 mice. Twenty-eight NOG-hCD34 mice, which were reconstituted from 7 separate individual cord blood donors, respectively, were inoculated with EBV via an intravenous injection between 13 and 16 weeks after hHSC transplantation. Large amounts of EBV DNA were first detected at 3 wpi and then plateaued until 10 wpi, at which time, all mice were killed for analysis (Figure 1A). EBV infection was fatal for most mice, and 71.4% of the infected mice either died or were killed because

of severe weight loss by 10 wpi (Figure 1B). Interestingly, during 5-7 wpi, 20 male mice infected with EBV showed greater viremia and died more rapidly than 8 EBV-infected female mice (Figure 1C).

Yajima and colleagues[21] have previously reported that humanized NOG mice (hNOG mice) infected with EBV died within 10 wpi. In their study, infected hNOG mice exhibited tumors containing EBV-positive B cells, which is consistent with EBV-associated B-cell lymphomas.[21] Therefore, we first set forward to look for signs of B-cell proliferative disorders in PB and organs of EBV-infected NOG-hCD34 mice. As shown in Figure 1D, however, B-cell expansion in PB was not found after EBV infection, whereas expansion of $CD8^+$ T cells was observed. Gross examination of spleen and liver of EBV-infected mice showed hepatosplenomegaly (Figure 1E). MNCs were isolated from spleen, liver, ascitic lavage, BM, and kidneys, and the number of $CD19^+$ B cells and $CD8^+$ T cells were determined by flow cytometry. If the EBV-infected NOG-hCD34 mice had B-cell proliferative disorder, this analysis would show drastic increase of $CD19^+$ B cells rather than $CD8^+$ T cells. However, flow cytometry revealed systemic organ infiltration by $CD8^+$ T cells in infected mice, as shown by a 10-fold increase in spleen and BM and a 100-fold increase in liver, lung, kidney, and ascitic lavage (Figure 1F). In contrast, the only organ that showed a significant increase in the number of B cells in infected mice was liver (Figure 1F). Moreover, immunostaining showed that the infiltrating and/or expanded cells in spleen and liver of EBV-infected mice primarily consisted of $CD8^+$ T cells and $CD68^+$ histiocytes, with occasional $CD20^+$ B cells (Figure 1G), and that B-cell tumors in infected mice were not detected. Taken together, these findings are inconsistent with B-cell proliferative disorders in EBV-infected NOG-hCD34 mice.

It is well known that EBV-associated malignant B-cell lymphomas are infected with EBV.[1] To assess the presence of EBV-infected cells in infected mice, in situ hybridization for EBERs, which are viral RNAs expressed in all EBV-infected cells,[1] was applied. As shown in Figure 1H, EBER-positive cells were detected in both spleen and liver of infected mice. However, the frequency of EBER-positive cells ($< 1/20$ of infiltrating lymphocytes) was lower than previously reported.[21] This result provides additional evidence that the B-cell proliferation caused by EBV infection in our study was modest and negligible. Taken together, these results strongly suggest that the EBV-infected NOG-hCD34 mice in our study died in a manner distinctly different from EBV-associated B-cell lymphoma-dependent death.

Hemophagocytosis in BM, spleen, and liver of EBV-infected NOG-hCD34 mice

The expansion of and infiltration by $CD8^+$ T cells together with the large number of histiocytes in spleen and liver (Figure 1D,F,G) prompted us to look into the immunopathology for the cause of the high mortality. HLH is a fatal immunopathologic condition that can be caused by EBV infection, and infiltration of $CD8^+$ T cells into multiple organs and histiocyte proliferation are common in patients with EBV-HLH.[1,3,5,15] Cardinal laboratory findings for HLH include hemophagocytosis, cytopenia, hypercytokinemia, and hyperferritinemia.[3] To explore this possibility, we set out to examine the presence of hemophagocytosis in BM of infected mice by NSE staining. As observed in both the spleen and liver of infected mice (Figure 1G), a large number of granule-containing histiocytes was detected in BM (Figure 2A). In addition, Giemsa staining revealed that these histiocytes contained multiple intracellular erythrocytes (Figure 2B). However, granule-residing and/or hemophagocytosed histiocytes were scarcely detected in BM of mock-infected mice (data not shown).

H&E staining confirmed that a large number of histiocytes resided in spleen and hepatic sinusoids of infected mice compared with those of mock-infected mice (Figure 2C), which supports the immunostaining result (Figure 1G). Moreover, Berlin blue staining revealed that these histiocytes in spleen and hepatic sinusoids of infected mice contained intracellular hemosiderin, which was derived from engulfed erythrocytes (Figure 2D). Taken together, these results demonstrate the presence of prominent hemophagocytosis in BM, spleen, and hepatic sinusoids of EBV-infected NOG-hCD34 mice.

Normocytic anemia and thrombocytopenia in EBV-infected NOG-hCD34 mice

Cytopenia of more than 2 kinds of blood cells such as erythrocytes and platelets is one of the current diagnostic criteria for HLH.[3] To investigate whether cytopenia occurred in EBV-infected mice, the PB of 10 EBV-infected and 7 mock-infected mice was routinely analyzed. As shown in Figure 3B-E and also summarized in Table 1, we found that the numbers of erythrocytes and platelets, hematocrit level, and hemoglobin concentration decreased in PB of EBV-infected mice, suggesting erythropenia and thrombocytopenia. However, the values of MCV, MCH, and MCHC in PB of EBV-infected mice were comparable with those in mock-infected mice (Figure 3F-H). These results directly indicate that normocytic anemia occurred in EBV-infected NOG-hCD34 mice.

In addition to the normocytic anemia, viremia (Figure 3A) and leukocytosis (Figure 3I), which was predominantly $CD8^+$ T cells (Figure 1D), also were observed in EBV-infected mice. Moreover, EBV-infected mice eventually showed severe weight loss (Figure 3J). To assess the time course of pathologic events observed in EBV-infected mice, the obtained results from 10 EBV-infected mice were summarized in Table 1. Interestingly, leukocytosis was firstly observed after the appearance of viremia (1.60 ± 0.48 weeks after viremia). Then, erythropenia, thrombocytopenia, and a decrease in hemoglobin were followed by leukocytosis (1.88 ± 0.48 weeks, 2.13 ± 0.72 weeks, and 2.14 ± 0.46 weeks after viremia, respectively). Finally, weight loss was detected (2.89 ± 0.65 weeks after viremia). Taken together, these results suggest that the normocytic anemia in EBV-infected mice occurred after EBV replication and leukocytosis, ultimately leading to a morbid condition.

Organ infiltration and aberrant IFN-γ production by activated non-EBV–specific $CD8^+$ T cells

Because $CD8^+$ T-cell activation is thought to play an important role in HLH pathogenesis,[3-5] the activation status of $CD8^+$ T cells in infected mice was analyzed. As shown in Figure 4A, $CD8^+$ T cells dramatically increased in PB after EBV infection. This increase was attributed to the expansion of $CD45RO^+$ memory subsets, and, in particular, $CD45RO^+CD38^+HLA\text{-}DR^+$ activated subsets (Figure 4C-D). $CD45RA^+$ naive $CD8^+$ T cells displayed no increase after infection (Figure 4B). Moreover, the numbers of the activated $CD8^+$ T cells isolated from all analyzed organs of infected mice increased at least 10-fold compared with those of mock-infected mice (Figure 4E). Furthermore, splenic $CD8^+$ T cells were stained for Ki67, a nuclear antigen expressed exclusively in proliferating/activated cells.[32] As shown in Figure 4F, the percentage of splenic $CD8^+$ T cells positive for Ki67 in EBV-infected mice was approximately 2-fold greater than that in mock-infected mice.

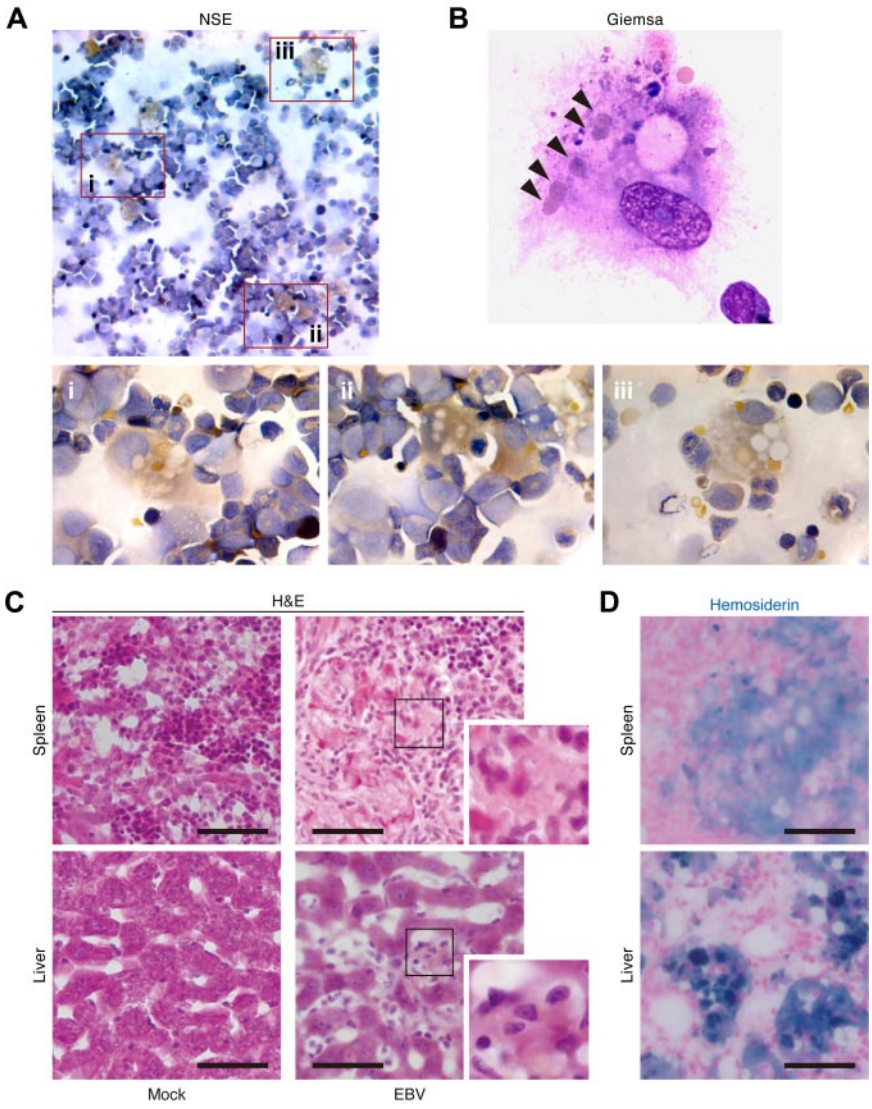

Figure 2. Hemophagocytosis in EBV-infected NOG-hCD34 mice. (A-B) Hemophagocytosis in the BM of EBV-infected mice. The specimens of the BM fluid smear of EBV-infected mice were prepared and assessed by NSE staining (A) and Giemsa staining (B). (A) NSE staining. Histiocytes (brown) and neutrophils (blue) were stained. Areas enclosed with squares (i-iii) indicate the histiocytes with granules and are, respectively, enlarged in panels i through iii. (B) Giemsa staining. A representative histiocyte with phagocytosis is shown. Arrowheads indicate engulfed erythrocytes. (C-D) Hemophagocytosis in the spleen and hepatic sinusoid of EBV-infected mice. Tissue sections were assessed by H&E staining (C) and Berlin blue staining (hemosiderin staining; D). (C) H&E staining. Representatives of spleen (top) and liver (bottom) of mock-infected mice (left) and EBV-infected mice (right) are shown. Areas enclosed with squares are enlarged in the bottom right of each panel and indicate morphologically activated histiocytes. (D) Berlin blue staining. Representatives of spleen (top) and liver (bottom) of EBV-infected mice are shown. Note that the cells stained with blue indicate hemosiderin-containing hemophagocytic histiocytes. Scale bars in panels C and D represent 50 μm.

Proinflammatory hypercytokinemia is another hallmark feature of HLH.[3] In addition, it is known that activated CD8$^+$ T cells can produce proinflammatory cytokines such as IFN-γ and TNF-α, which promote activation/proliferation of CD8$^+$ T cells and histiocytes.[3-6,12,13] To investigate this issue, the expression levels of *IFNG* (encodes IFN-γ) and *TNFA* (encodes TNF-α) in splenic CD8$^+$ T cells of EBV-infected and mock-infected mice were assessed. As shown in Figure 4G, *IFNG* was significantly elevated in CD8$^+$ T cells of infected mice, whereas *TNFA* was not. Next, the concentrations of IFN-γ and TNF-α in plasma were longitudinally assessed. A significant elevation of plasma IFN-γ concentration in infected mice was first detected at 4 wpi and was maintained at a high level (Figure 4H). In contrast, plasma TNF-α concentrations in infected mice were almost comparable with those in mock-infected mice (Figure 4I). Furthermore, to assess the dynamics of virus replication, CD8$^+$ T-cell activation, and IFN-γ hypercytokinemia in EBV-infected mice, the obtained results from 8 EBV-infected mice were summarized in Table 2. It is worth noting that the activation/expansion of CD8$^+$ T cells in PB and the elevation of plasma IFN-γ concentrations were first detected just after the appearance of viremia and occurred concurrently (0.38 ± 0.18 weeks and 0.50 ± 0.19 weeks after viremia, respectively). These findings suggest that CD8$^+$ T-cell activation and IFN-γ hypercytokinemia are elicited after EBV replication.

Because it has been known that EBV-specific HLA-restricted CTLs are easily induced by EBV infection,[1,33] the activation of CD8$^+$ T cells found in our EBV-infected mice may be because of a specific immune response against EBV antigens. To assess the immunologic specificity of the activated CD8$^+$ T cells against EBV, we isolated splenic human MNCs from 7 EBV-infected and 4 mock-infected mice. These mice underwent transplantation with hHSCs possessing HLA-A*2402 (supplemental Table 1), which is one of the dominant HLA class I alleles for EBV antigen presentation.[34] Specificity of the CD8$^+$ T cells for EBV antigens was evaluated by the use of HLA-A*2402 tetramers coupled with 5 different EBV peptides. HLA-A*2402 tetramers coupled with HIV-1 peptides were used as a negative control. As shown in Figure 4J, we detected HLA-A*2402–restricted EBV-specific CD8$^+$ T cells only in EBV-infected mice, although the frequency was quite low (0.22% ± 0.09%).[33] However, HLA-A*2402–restricted HIV-1–specific CD8$^+$ T cells were not found (Figure 4J). These results suggest that the expansion of activated CD8$^+$ T cells was not directly because of EBV-specific antigen recognition.

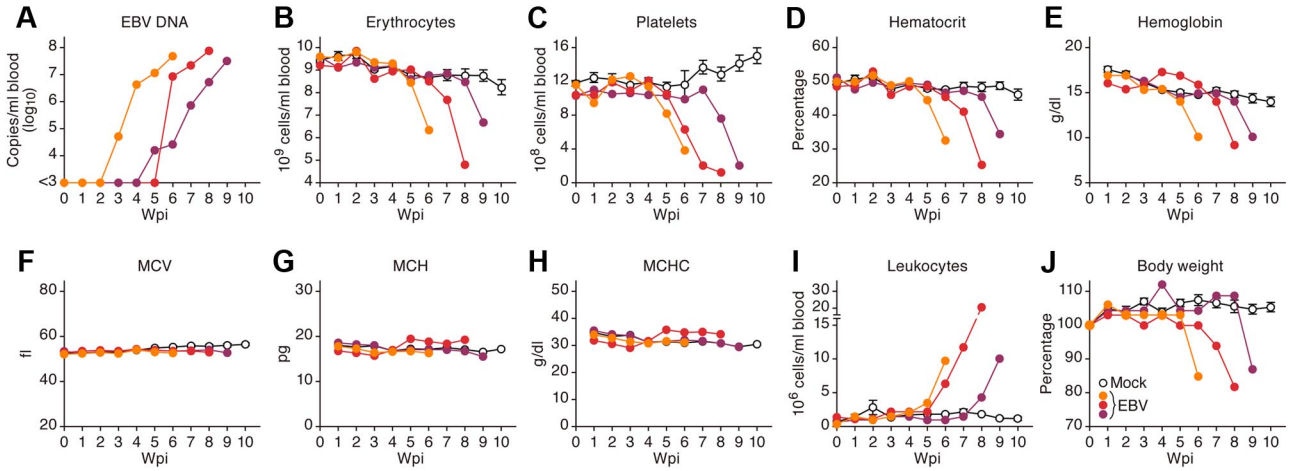

Figure 3. Viremia, normocytic anemia, thrombocytopenia, leukocytosis, and severe weight loss in EBV-infected NOG-hCD34 mice. (A) EBV load in the PB of 3 representative EBV-infected mice. (B-I) Longitudinal analyses of hematopoietic cells in PB. PB was routinely collected from mock-infected and EBV-infected mice, and the numbers of erythrocytes (B), platelets (C), and leukocytes (I) were measured by hematometry. Hematocrit (D), hemoglobin concentration (E), and the values of MCV (F), MCH (G), and MCHC (H) were also measured by hematometry. (J) Change on body weight. The body weights of mock-infected and EBV-infected mice were routinely measured and are shown as the ratio to the initial weight. Results from mock-infected mice (n = 7) are presented in means ± SEM, and representative results of 3 EBV-infected mice are, respectively shown. Each color represents the result from an identical EBV-infected mouse.

Relevance of EBV load, IFN-γ hypercytokinemia, and CD8$^+$ T-cell activation in respect to the morbid condition in EBV-infected NOG-hCD34 mice

It is known that EBV rarely infects T cells and can cause a T-cell proliferative disorder.[1,3,11,35] This disorder is known as chronic active EBV infection (CAEBV) and HLH can be accompanied by CAEBV.[1,3,11,35] To assess whether T cells are infected with EBV in NOG-hCD34 mice, splenic MNCs were sorted into human CD4$^+$, CD8$^+$, CD19$^+$, and murine CD45$^+$ fractions and the amount of EBV DNA in each fraction was quantified. When the murine CD45$^+$ fraction was used as the background control, no significant amount of EBV DNA was detected in human CD4$^+$ and CD8$^+$ fractions (Figure 5A). However, a large amount of EBV DNA (> 70 copies/cell) was detected in human CD19$^+$ B-cell fraction (Figure 5A). Although it is known that EBV infection in T cells induce the proliferation of the infected cell,[1,3,11,35] the number of EBER-positive cells was small (Figure 1H), and the level of viral DNA in either CD4$^+$ T cells or CD8$^+$ T cells was comparable with that of the background sample (Figure 5A). Therefore, these results suggest that the EBV-associated T-cell proliferative disorder is not likely caused in infected mice and that the pathogenesis observed in EBV-infected NOG-hCD34 mice is distinct from CAEBV-like disorder.

MNCs were isolated from spleen, liver, ascitic lavage, BM, and kidneys, and the amount of viral DNA was assessed. As shown in Figure 5B, large amounts of EBV DNA were detected in all organs assessed, showing systemic and productive replication of EBV. In addition, immunostaining revealed the expression of lytic viral proteins, ZEBRA (derived from *bzlf1*), and gp110 (derived from *balf4*), in both spleen and liver (Figure 5C). Moreover, RT-PCR revealed that not only latent viral genes (*lmp1*, *lmp2a*, and *ebna2a*) but also lytic viral genes (*bzlf1*, *balf2*, *bxlf1*, *barf1*, *bclf1*, and *bllf1*) were expressed in spleen of infected mice (Figure 5D). These results demonstrate that productive EBV replication takes place in infected NOG-hCD34 mice.

Clinical studies have shown that patients with EBV-HLH and a high viral load go on to have a worse prognosis than those with a

Table 1. Summary of the time points when hematologic disorders and severe weight loss were first observed*

Mouse no.†	VL‡	Leukocytosis§¶	Erythropenia§‖	Thrombocytopenia§‖	HGB decrease§‖	Weight loss§‖
Mouse 1	5	7 (+2)	6 (+1)	6 (+1)	6 (+1)	9 (+4)
Mouse 2	5	8 (+3)	9 (+4)	8 (+3)	9 (+4)	9 (+4)
Mouse 3	3	8 (+5)	–	9 (+6)	–	10 (+7)
Mouse 4	4	5 (+1)	6 (+2)	–	6 (+2)	–
Mouse 5	5	6 (+1)	6 (+1)	8 (+3)	8 (+3)	8 (+3)
Mouse 6	3	3 (± 0)	3 (± 0)	3 (± 0)	4 (+1)	4 (+1)
Mouse 7	3	5 (+2)	6 (+3)	6 (+3)	6 (+3)	6 (+3)
Mouse 8	4	5 (+1)	–	5 (+1)	–	5 (+1)
Mouse 9	6	6 (± 0)	7 (+1)	6 (± 0)	7 (+1)	7 (+1)
Mouse 10	7	8 (+1)	10 (+3)	–	–	9 (+2)
Average ± SEM**	–	1.60 ± 0.48	1.88 ± 0.48	2.13 ± 0.72	2.14 ± 0.46	2.89 ± 0.65

HGB indicates hemoglobin; VL, viral load; and wpi, weeks postinfection.
*The time points when infected mice showed significant differences to mock-infected mice are presented as wpi.
†The results from mice no. 2, 7, and 9 are shown in Figure 3.
‡The wpi when EBV DNA was firstly detected is presented.
§The values in parentheses represent the difference of each parameters to VL.
¶The wpi when the value was more than the average of mock-infected mice + SD is presented.
‖The wpi when the value was more than the average of mock-infected mice − SD is presented.
**The differences to VL (represented in parentheses) are summarized and presented as average ± SEM.

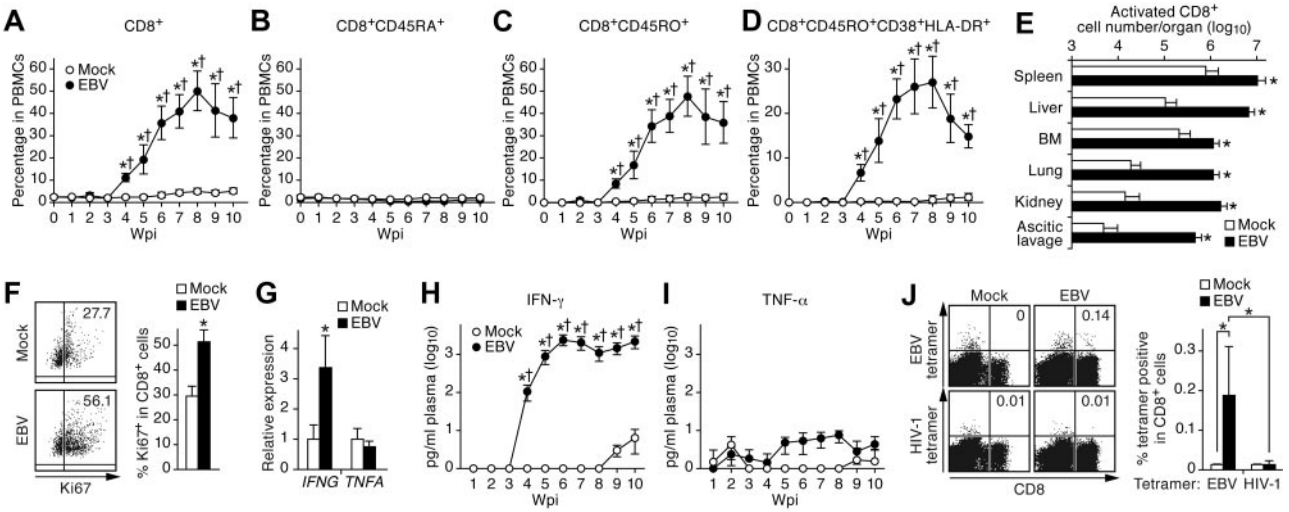

Figure 4. Expansion and activation of CD8⁺ T cells and IFN-γ hypercytokinemia in EBV-infected NOG-hCD34 mice. (A-D) Dynamics of human CD8⁺ T cells in PB. PB was routinely collected from mock-infected mice (n = 5) and EBV-infected mice (n = 12) and was analyzed by flow cytometry. Percentages of CD8⁺ cells (A), CD8⁺CD45RA⁺ cells (B), CD8⁺CD45RO⁺ cells (C), and CD8⁺CD45RO⁺CD38⁺HLA-DR⁺ cells (D) in PBMCs are, respectively shown. (E) Expansion of activated CD8⁺ T cells in multiple organs of EBV-infected mice. The cell numbers of CD8⁺CD45RO⁺CD38⁺HLA-DR⁺ cells (activated CD8⁺ T cells) in the spleen, liver, BM, lung, kidney, and ascitic lavage fluid of mock-infected mice (n = 4) and EBV-infected mice (n = 7) are shown. (F) Ki67 expression in CD8⁺ T cells. (Left) Representatives of splenic CD8⁺ T cells of mock-infected and EBV-infected mice. Values on quadrants represent the percentages of CD8⁺ T cells positive for Ki67. (Right) The percentages of Ki67⁺ cells in splenic CD8⁺ T cells of mock-infected mice (n = 4) and EBV-infected mice (n = 7) are shown. (G) mRNA expression in CD8⁺ T cells. Splenic CD8⁺ T cells of mock-infected mice (n = 6) and EBV-infected mice (n = 9) were isolated by cell sorting. The expression levels of *IFNG* (left) and *TNFA* (right) were analyzed by real-time RT-PCR and were normalized to that of *GAPDH*. Results are presented as the fold change compared with the value in mock-infected mice. (H-I) Longitudinal quantification of IFN-γ and TNF-α in plasma. Plasma was routinely collected from mock-infected mice (n = 4) and EBV-infected mice (n = 7), and the concentrations of IFN-γ (H) and TNF-α (I) were quantified by cytokine bead array system. (J) Detection of EBV-specific HLA-A*2402–restricted CD8⁺ cells. Splenic human MNCs isolated from mock-infected mice (n = 4) and EBV-infected mice (n = 7) were stained with an anti-CD8 antibody and either HLA-A*2402 EBV tetramers or HLA-A*2402 HIV-1 tetramers (as a negative control of the assay) and were analyzed by flow cytometry. Representatives (left) and the percentages of CD8⁺ T cells positive for the tetramers in mock-infected and EBV-infected mice (right) are shown. Asterisks in panels A, C, D, and H represent statistic significance ($P < .05$ by Student *t* test) versus the value obtained from the mock-infected mice, and daggers represent statistic significance ($P < .05$ by paired *t* test) vs the initial value. Asterisks in panel E represent statistic significance ($P < .05$ by Welch *t* test) versus the value obtained from the mock-infected mice. Asterisks in panel F, G, and J represent statistic significance ($P < .05$ by Student *t* test) versus the value obtained from the mock-infected mice.

low viral load.[4] To investigate whether the relevance between viral load and immune activation is observed in our model, we compared the level of EBV DNA and IFN-γ concentration in plasma and Ki67 expression in splenic CD8⁺ T cells to one another in each infected mouse. As shown in Figure 5E, the percentage of Ki67⁺ cells in splenic CD8⁺ T cells significantly correlated with the concentration of IFN-γ in plasma. In addition, we found that the EBV load in plasma positively and significantly correlated with both the percentage of splenic Ki67⁺CD8⁺ T cells (Figure 5F) and plasma IFN-γ concentration (Figure 5G). Moreover, the infected mice that were killed before 10 wpi because of severe weight loss tended to exhibit greater amounts of EBV DNA copies, IFN-γ concentrations, and Ki67 expression in CD8⁺ T cells than the infected mice that survived until 10 weeks (Figures 5E-G).

Table 2. Summary of the time points when immunologic disorders and severe weight loss were first observed*

Mouse no.	VL†	Activated CD8‡§	IFN-γ†¶	Weight loss§‖
Mouse 11	4	4 (± 0)	4 (± 0)	–
Mouse 12	4	4 (± 0)	4 (± 0)	6 (+2)
Mouse 13	3	4 (+1)	4 (+1)	6 (+3)
Mouse 14	4	4 (± 0)	4 (± 0)	9 (+5)
Mouse 15	3	3 (± 0)	4 (+1)	8 (+5)
Mouse 16	4	4 (± 0)	4 (± 0)	–
Mouse 17	3	4 (+1)	4 (+1)	6 (+3)
Mouse 18	3	4 (+1)	4 (+1)	5 (+2)
Average ± SEM**	–	0.38 ± 0.18	0.50 ± 0.19	3.33 ± 0.56

VL indicates viral load; and wpi, weeks postinfection.

*The time points when infected mice showed significant differences to mock-infected mice are presented as wpi.

†The wpi when EBV DNA was firstly detected is presented.

‡The values in parentheses represent the difference of each parameters to VL.

§The wpi when the parcentage CD8⁺CD45RO⁺CD38⁺HLA-DR⁺ cells in PBMCs of each infected mouse was more than the average of that of mock-infected mice + SD is presented.

¶The wpi when the concentration of IFN-γ in plasma of each infected mouse was more than the average of mock-infected mice + SD is presented.

‖The wpi when the value was more than the average of mock-infected mice − SD is presented.

**The differences to VL (represented in parentheses) are summarized and presented as average ± SEM.

Decrease in the number of natural killer cells, myeloid dendritic cells, and plasmacytoid dendritic cells in the spleen and EBER1 detection in the plasma of EBV-infected mice

To further investigate the dynamics of EBV-HLH–like disorders in infected mice, we assessed the proportion of human leukocytes in the spleen. As shown in Figure 6A, the numbers of naive, memory, and regulatory CD4⁺ T cells in the spleen of infected mice were comparable with those in mock-infected mice. However, we found a significant decrease in the number of natural killer (NK) cells, myeloid dendritic cells (MDCs), and plasmacytoid dendritic cells (PDCs) in the spleen of infected mice (Figure 6B-C). Moreover, we quantified the concentration of IFN-β in the plasma of infected mice and found that the level of IFN-β in infected mice was comparable with that in mock-infected mice (Figure 6D). Furthermore, the level of IFN-β in plasma did not correlate with the levels of EBV DNA, IFN-γ concentration, or Ki67 expression in CD8⁺ T cells (data not shown). These data suggest that IFN-β is not associated with the progression of the EBV-HLH–like disorder.

It was also reported that high levels of EBER1 were detected in plasma or sera of EBV-HLH patients.[31] We quantified the amount of EBER1 in the plasma of 14 infected mice and found that high

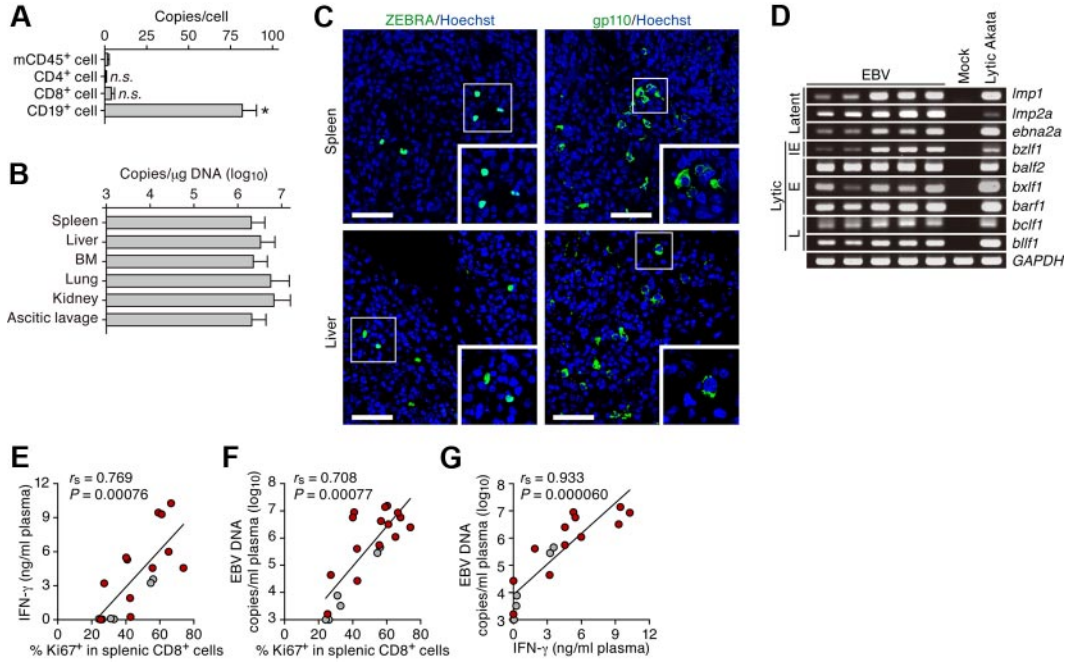

Figure 5. Productive EBV replication and the relevance between EBV infection and immune activation in infected NOG-hCD34 mice. (A) Distribution of EBV DNA in splenic human MNCs. Splenic MNCs were isolated from EBV-infected mice (n = 7), and human leukocytes (CD4$^+$, CD8$^+$, and CD19$^+$ cells, respectively) and murine CD45$^+$ leukocytes (mCD45$^+$ cells, as the background control) were separated by cell sorting. Results are presented in EBV copies per cell of each cell populations. Asterisk represents statistic significance ($P < .05$ by Student *t* test) versus the value obtained from mCD45$^+$ cells. n.s. indicates no statistical significance. (B) Systemic EBV replication in multiple organs. DNA was extracted from the human MNCs that were isolated from spleen, liver, BM, lung, kidney, and ascitic lavage fluid of EBV-infected mice (n = 7), and the copy number of EBV DNA was measured. (C) Immunostaining for ZEBRA and gp110. Representatives of spleen (top) and liver (bottom) of EBV-infected mice are shown. ZEBRA and gp110 were shown in green, and nuclei were shown in blue by staining with Hoechst. Areas enclosed with squares are enlarged in bottom right of each panel. Scale bars represent 50 μm. (D) Expression of EBV genes. RNA was extracted from splenic human MNCs of 5 EBV-infected mice, a mock-infected mouse, and anti-IgG–stimulated Akata cells ("Lytic Akata"), and the expression of EBV latent genes (*lmp1*, *lmp2a*, and *ebna2a*) and EBV lytic genes (*bzlf1*, *balf2*, *bxlf1*, *barf1*, *bclf1*, and *bllf1*) was determined by RT-PCR. As the internal control, *GAPDH* expression was also determined. IE indicates immediate early gene; E, early genes; and L, late genes. (E-G) Correlation between viral load in plasma, activation frequency of CD8$^+$ T cells, and the level of IFN-γ in plasma. The percentage of Ki67$^+$ cells in splenic CD8$^+$ T cells (x-axis) and the concentration of IFN-γ in plasma (y-axis; E), the percentage of Ki67$^+$ cells in splenic CD8$^+$ T cells (x-axis) and EBV DNA copies in plasma (y-axis; F), and the concentration of IFN-γ in plasma (x-axis) and EBV DNA copies in plasma (y-axis; G) are, respectively shown. Red dots represent the results from the EBV-infected mice exhibited severe weight loss and were killed before 10 wpi (n = 13), whereas gray dots represent the results from the EBV-infected mice survived until 10 wpi (n = 5). The lines present exponential approximation. Spearman rank correlation coefficient (r_s) was adopted to determine statistically significant correlation between each value.

levels of EBER1 were detected in 8 infected mice (Figure 6E). Notably, the level of EBER1 in plasma of infected mice was almost comparable with or greater than that of patients.[31] However, the level of EBER1 in plasma did not correlate with disease severity and the clinical/laboratory features of disease (data not shown).

Discussion

To simulate EBV pathogenesis in vivo, several experimental animal models have been established.[36-41] In addition, hHSC-transplanted humanized mouse models have been used for EBV studies.[16-21] In this study, we established a novel humanized mouse model of EBV infection. NOG-hCD34 mice, which were newborn NOG mice transplanted with hHSCs, displayed a condition that has a different pathology from B-cell lymphomas when infected with EBV. Further investigations of EBV-infected NOG-hCD34 mice demonstrated the following: (1) hepatosplenomegaly; (2) CD8$^+$ T-cell activation and organ infiltration; (3) IFN-γ hypercytokinemia; (4) normocytic anemia; (5) thrombocytopenia; (6) histiocyte proliferation; and (7) hemophagocytosis in BM, spleen, and liver. These 7 features displayed by EBV-infected NOG-hCD34 mice are strongly indicative of EBV-HLH. To the best of our knowledge, this is the first report demonstrating the pathogenesis of EBV-HLH in an animal model. In addition to the establishment of a novel model for EBV-HLH, we also found a significant correlation between viral replication and hyperimmune activation in infected mice. Furthermore, a significant decrease of type I IFN-producing cells such as MDCs, PDCs, and NK cells was observed in spleen of infected mice. Taken together, these findings suggest that productive EBV replication induces hyperactivation of CD8$^+$ T cells, and that the breakdown of balanced immunity associates with disease progression.

Murine models of congenital HLH have shed light on the pathogenesis of this poorly understood disorder.[12,13] For instance, *Prf* knockout mice developed HLH after LCMV infection, resulting in the death of most infected mice.[12] Interestingly, the importance of CD8$^+$ T-cell activation and IFN-γ on the pathogenesis of HLH was also suggested in the same study.[12] As previously reported,[3-6,12,13] we found an augmented expression of *IFNG* in splenic CD8$^+$ T cells of EBV-infected mice. In addition, we found that the activation/expansion of CD8$^+$ T cells in PB and IFN-γ cytokinemia occurred concurrently in infected mice (Table 2), suggesting that CD8$^+$ T-cell activation and IFN-γ production take place in an orchestrated and synergistic manner in EBV-infected mice. After the expansion of CD8$^+$ T cells and IFN-γ hypercytokinemia, normocytic anemia and thrombocytopenia were subsequently observed (Table 1). In fact, it was reported that proinflammatory cytokines, including IFN-γ, have the potential to activate macrophages/histiocytes and trigger hemophagocytosis both in vitro[42] and in vivo.[8,33] Our results suggest that overproduced IFN-γ elicited histiocyte activation, leading to hemophagocytosis and

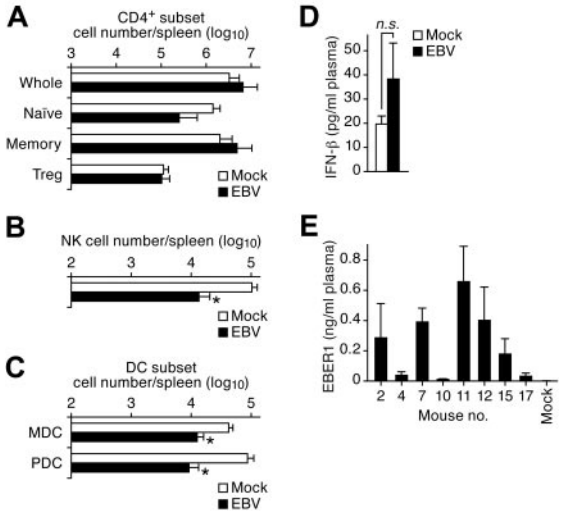

Figure 6. Decrease in the number of NK cells, MDCs, and PDCs and the detection of EBER1 and type I IFN in the plasma of infected NOG-hCD34 mice. (A-C) Human MNC numbers in spleen. The cell numbers of $CD4^+$ T-cell subset (whole, $CD4^+CD45^+$; naive, $CD4^+CD45RA^+CD45^+$; memory, $CD4^+CD45RO^+CD45^+$; Treg, $CD4^+FOXP3^+CD45^+$; A), NK cell ($CD56^+CD3^-CD45^+$; B), and DC subset (MDC, $Lineage^-[CD3^-CD14^-CD19^-CD56^-CD303^-]HLA\text{-}DR^{high}CD11c^{high}CD45^+$; PDC, $CD303^+CD45^+$; C) in spleen of mock-infected mice ($n = 6$) and EBV-infected mice ($n = 6$) are shown. Asterisks represent statistic significance ($P < .05$ by Welch t test) versus the value obtained from the mock-infected mice. (D) Quantification of IFN-β in plasma. The concentration of IFN-β in the plasma of mock-infected mice ($n = 5$) and EBV-infected mice ($n = 14$) was quantified by ELISA. n.s. indicates no statistical significance. (E) Quantification of EBER1 in plasma. The concentration of EBER1 in plasma of 8 EBV-infected mice and a mock-infected mouse was quantified as previously described.[31] The mouse numbers correspond with those in Tables 1 and 2.

anemia, and that $CD8^+$ T cells and IFN-γ played a pivotal role in promoting HLH.

In contrast to IFN-γ, type I IFNs (eg, IFN-β) are well-known to possess the robust potential to suppress virus replication, including EBV.[43] Recently, Iwakiri et al[31] have documented that EBER1 released from EBV-infected cells stimulates MDCs in a Toll-like receptor 3 (TLR3)–dependent manner and induces type I IFN production. In addition to MDCs, it was reported that NK cells also express TLR3 and are activated by TLR3 ligands.[44] Moreover, PDCs are involved in anti-EBV immunity by the secretion of type I IFN through TLR9 pathways.[43] These reports suggest that type I IFN produced by NK cells, MDCs, and PDCs through TLR3 and/or TLR9 signaling has the potential to suppress EBV-associated immunopathologic disorders. However, we found that NK cells, MDCs, and PDCs in the spleen of infected mice were severely decreased. Furthermore, we did not observe IFN-β hypercytokinemia in infected mice. These findings suggest that the depletion of type I IFN-producing cells such as NK cells, MDCs, and PDCs resulted in the absence of the induction of type I IFN production, which contributes to the progression of the EBV-HLH-like disorder in infected NOG-hCD34 mice.

Although the initial trigger of the $CD8^+$ T-cell activation causing the hyperimmune state in our EBV-infected mouse model remains unclear, several plausible explanations include direct and/or indirect $CD8^+$ T-cell activation by EBV-derived ligands. Reinforcing this assumption was our finding of a low frequency[33] of HLA-A*2402–restricted EBV-specific CTLs in the spleen of infected NOG-hCD34 mice, although their levels were comparable with previous reports.[18,20,21] In addition, TLR3 is expressed on $CD8^+$ T cells and induces a signaling cascade in these cells resulting in IFN-γ secretion without enhancing CTL activity.[45] As mentioned previously, EBER1 is able to trigger TLR3 signaling, and we detected high levels of EBER1 in the plasma of EBV-infected NOG-hCD34 mice at amounts comparable with EBV-infected patients (Figure 6E).[31] Therefore, it is possible that EBER1/TLR3 signaling in $CD8^+$ T cells may be one of the triggers to induce IFN-γ hypercytokinemia. Furthermore, when NOG-hCD34 mice were inoculated with heat-inactivated EBV, an absence of viremia, hyperimmune activation, anemia, and severe weight loss were observed (data not shown), suggesting that the agent(s) that triggered the hyperimmune activation in infected mice are derived from EBV replication. Moreover, we found that EBV DNA was detected in PB before $CD8^+$ T-cell activation and that the level of plasma EBV load positively correlated with the level of $CD8^+$ T-cell activation. In fact, a clinical study reported that EBV-HLH patients with a high viremia tend to exhibit a worse prognosis than those with a low viremia.[4] Therefore, our data suggest that productive EBV replication is essential for hyperactivation of $CD8^+$ T cells, which can lead to severe disorders.

In contrast to the EBV-infected humanized NOG mice displaying the EBV-HLH phenotype shown in our study, similar EBV-infected humanized NOG mice have exhibited EBV-associated B-cell proliferative disorders.[20,21] The different disease outcomes may be attributed to the different experimental approaches taken in conducting the studies. For instance, we used 20 male and 8 female NOG mice as hHSC recipients and found that the male mice exhibited higher levels of viremia and died more rapidly than female mice (Figure 1C). However, the previous studies used only female NOG mice as hHSC recipients.[20,21] Why male mice were more susceptible to a fatal outcome is unclear, however, a previous study has also observed a similar effect. Transgenic mice expressing hepatitis C virus core proteins had severe disorders and greater mortality in male transgenic mice compared with female transgenic mice.[46] Therefore, it is conceivable that the sex difference of the recipient NOG mice may be one of the underlying reasons why our findings varied from previous studies.[20,21] In addition, it was reported that their hNOG mice seem to have the potential to reproduce humoral immune responses against EBV[21] and HIV-1.[47] However, we have previously shown that our NOG-hCD34 mice were not capable of producing antibodies against HIV-1[25] and are unlikely to produce antibodies against EBV (data not shown). Thus, the difference in the potential of humoral immunity may also play a role in the EBV pathogenesis. Moreover, it is worth noting that EBV-HLH is a disease that tends to develop in children and young adults.[1,4] In this study, we transplanted hHSCs into newborn NOG mice and inoculated them with EBV at a relatively younger age period (13-16 weeks of age). However, the authors of the previous study used older NOG mice for hHSC transplantation and inoculated them with EBV at relatively older ages (20-38 weeks of age).[20,21] Because the age for EBV infection appears to be one of the critical determinants for the development of EBV-HLH in humans,[1,4] the difference in the age of humanized mice used for EBV infection may be a plausible explanation for the different pathologic outcomes caused by EBV infection. Overall, our system is more adept to simulate and reflect EBV-HLH pathogenesis in a manner relevant to what is observed humans compared with the previous study.

In conclusion, the model of acquired HLH we have generated in our humanized NOG mice will provide us with clues to elucidate how HLH is caused by EBV infection. Moreover, our model can also be used to develop and evaluate novel therapies targeting EBV-HLH. On the basis of not only on the current data, but on previous murine studies,[12,13] depletion of $CD8^+$ T cells as well as

neutralization of IFN-γ might prove useful in amelioration of disease. Furthermore, it will be interesting to evaluate the effects of B-cell–depleting antibodies on disease progression.

Acknowledgments

We thank Tomoko Kobayashi, Peter Gee, and Kenji Sugata (Institute for Virus Research, Kyoto University); Takeshi Sairenji (Tottori University); Hiroshi Kimura (Nagoya University Graduate School of Medicine); Kouichi Ohshima (School of Medicine, Kurume University); and Kinya Nagata (Bio Medical Laboratories Inc) for their generous help in our study. We would like to express our appreciation for Ms Kotubu Misawa's dedicated support.

This work was supported in part by Grants-in-Aid for Scientific Research (B21390137, S22220007 to Y.K.) from the Japan Society for the Promotion of Science; a Grant-in-Aid for Scientific Research on Priority Areas "Matrix of Infection Phenomena" (18073008 to Y.K.) from the Ministry of Education, Culture, Sports, Science and Technology of Japan; Research on Emerging and Re-emerging Infectious Diseases, and Research on HIV/AIDS from the Ministry of Health, Labor and Welfare of Japan; and the Naito Foundation (to Y.K.). K.S. was supported by Research Fellowships of the Japan Society for the Promotion of Science for Young Scientists.

Authorship

Contribution: K.S. and Y.K. designed the research; K.S., N.M., C.N., Y.S., D.I., R.T., and K.K. performed experiments; K.S., N.M., and M.I. constructed and maintained NOG-hCD34 mice; K.S., N.M., C.N., Y.S., D.I., M.M., R.T., and K.T. analyzed results; K.S. and C.N. designed the figures; and K.S., C.N., K.T., and Y.K. wrote the paper.

Conflict-of-interest disclosure: The authors declare no competing financial interests.

Correspondence: Yoshio Koyanagi, Laboratory of Virus Pathogenesis, Institute for Virus Research, Kyoto University, 53 Shogoinkawara-cho, Sakyo-ku, Kyoto, Kyoto 606-8507, Japan; e-mail: ykoyanag@virus.kyoto-u.ac.jp.

References

1. Rickinson AB, Kieff E. Epstein-Barr virus. In: Knipe DM, Howley PM, eds. *Fields Virology*. Vol. 2 (5th ed). Philadelphia, PA: Lippincott Williams & Wilkins; 2007:2655-2700.
2. Cohen JI. Epstein-Barr virus infections, including infectious mononucleosis. In: Braunwald E, Fauci AS, Kasper DL, et al, eds. *Harrison's Principals of Internal Medicine*. Vol. 1 (15th ed) New York, NY: McGraw-Hill; 2001:1109-1111.
3. Kasahara Y, Yachie A, Takei K, et al. Differential cellular targets of Epstein-Barr virus (EBV) infection between acute EBV-associated hemophagocytic lymphohistiocytosis and chronic active EBV infection. *Blood.* 2001;98(6):1882-1888.
4. Rouphael NG, Talati NJ, Vaughan C, Cunningham K, Moreira R, Gould C. Infections associated with haemophagocytic syndrome. *Lancet Infect Dis.* 2007; 7(12):814-822.
5. Su IJ, Chen RL, Lin DT, Lin KS, Chen CC. Epstein-Barr virus (EBV) infects T lymphocytes in childhood EBV-associated hemophagocytic syndrome in Taiwan. *Am J Pathol.* 1994;144(6):1219-1225.
6. Créput C, Galicier L, Buyse S, Azoulay E. Understanding organ dysfunction in hemophagocytic lymphohistiocytosis. *Intensive Care Med.* 2008; 34(7):1177-1187.
7. Janka GE. Hemophagocytic syndromes. *Blood Rev.* 2007;21(5):245-253.
8. Stepp SE, Dufourcq-Lagelouse R, Le Deist F, et al. Perforin gene defects in familial hemophagocytic lymphohistiocytosis. *Science.* 1999; 286(5446):1957-1959.
9. Coffey AJ, Brooksbank RA, Brandau O, et al. Host response to EBV infection in X-linked lymphoproliferative disease results from mutations in an SH2-domain encoding gene. *Nat Genet.* 1998; 20(2):129-135.
10. Rigaud S, Fondaneche MC, Lambert N, et al. XIAP deficiency in humans causes an X-linked lymphoproliferative syndrome. *Nature.* 2006; 444(7115):110-114.
11. Dupré L, Andolfi G, Tangye SG, et al. SAP controls the cytolytic activity of CD8+ T cells against EBV-infected cells. *Blood.* 2005;105(11):4383-4389.
12. Jordan MB, Hildeman D, Kappler J, Marrack P. An animal model of hemophagocytic lymphohistiocytosis (HLH): CD8+ T cells and interferon gamma are essential for the disorder. *Blood.* 2004;104(3):735-743.
13. Wu C, Nguyen KB, Pien GC, et al. SAP controls T cell responses to virus and terminal differentiation of TH2 cells. *Nat Immunol.* 2001;2(5):410-414.
14. Brown DE, McCoy MW, Pilonieta MC, Nix RN, Detweiler CS. Chronic murine typhoid fever is a natural model of secondary hemophagocytic lymphohistiocytosis. *PLoS ONE.* 2010;5(2):e9441.
15. Risdall RJ, McKenna RW, Nesbit ME, et al. Virus-associated hemophagocytic syndrome: a benign histiocytic proliferation distinct from malignant histiocytosis. *Cancer.* 1979;44(3):993-1002.
16. Islas-Ohlmayer M, Padgett-Thomas A, Domiati-Saad R, et al. Experimental infection of NOD/SCID mice reconstituted with human CD34+ cells with Epstein-Barr virus. *J Virol.* 2004;78(24):13891-13900.
17. Melkus MW, Estes JD, Padgett-Thomas A, et al. Humanized mice mount specific adaptive and innate immune responses to EBV and TSST-1. *Nat Med.* 2006;12(11):1316-1322.
18. Strowig T, Gurer C, Ploss A, et al. Priming of protective T cell responses against virus-induced tumors in mice with human immune system components. *J Exp Med.* 2009;206(6):1423-1434.
19. Traggiai E, Chicha L, Mazzucchelli L, et al. Development of a human adaptive immune system in cord blood cell-transplanted mice. *Science.* 2004; 304(5667):104-107.
20. Yajima M, Imadome K, Nakagawa A, et al. T cell-mediated control of Epstein-Barr virus infection in humanized mice. *J Infect Dis.* 2009;200(10):1611-1615.
21. Yajima M, Imadome KI, Nakagawa A, et al. A new humanized mouse model of Epstein-Barr virus infection that reproduces persistent infection, lymphoproliferative disorder, and cell-mediated and humoral immune responses. *J Infect Dis.* 2008;198(5):673-682.
22. Ito M, Hiramatsu H, Kobayashi K, et al. NOD/SCID/gammacnull mouse: an excellent recipient mouse model for engraftment of human cells. *Blood.* 2002;100(9):3175-3182.
23. Nie C, Sato K, Misawa N, et al. Selective infection of CD4+ effector memory T lymphocytes leads to preferential depletion of memory T lymphocytes in R5 HIV-1-infected humanized NOD/SCID/IL-2Rgammanull mice. *Virology.* 2009;394(1):64-72.
24. Sato K, Izumi T, Misawa N, et al. Remarkable lethal G-to-A mutations in vif-proficient HIV-1 provirus by individual APOBEC3 proteins in humanized mice. *J Virol.* 2010;84(18):9546-9556.
25. Sato K, Nie C, Misawa N, Tanaka Y, Ito M, Koyanagi Y. Dynamics of memory and naive CD8+ T lymphocytes in humanized NOD/SCID/IL-2Rgammanull mice infected with CCR5-tropic HIV-1. *Vaccine.* 2010;28(suppl 2):B32-37.
26. Shimizu N, Yoshiyama H, Takada K. Clonal propagation of Epstein-Barr virus (EBV) recombinants in EBV-negative Akata cells. *J Virol.* 1996; 70(10):7260-7263.
27. Sato K, Aoki J, Misawa N, et al. Modulation of human immunodeficiency virus type 1 infectivity through incorporation of tetraspanin proteins. *J Virol.* 2008;82(2):1021-1033.
28. Sato K, Yamamoto SP, Misawa N, Yoshida T, Miyazawa T, Koyanagi Y. Comparative study on the effect of human BST-2/Tetherin on HIV-1 release in cells of various species. *Retrovirology.* 2009;6:53.
29. Miura Y, Misawa N, Maeda N, et al. Critical contribution of tumor necrosis factor-related apoptosis-inducing ligand (TRAIL) to apoptosis of human CD4+ T cells in HIV-1–infected hu-PBL-NOD-SCID mice. *J Exp Med.* 2001;193(5):651-659.
30. Jebbink J, Bai X, Rogers BB, Dawson DB, Scheuermann RH, Domiati-Saad R. Development of real-time PCR assays for the quantitative detection of Epstein-Barr virus and cytomegalovirus, comparison of TaqMan probes, and molecular beacons. *J Mol Diagn.* 2003;5(1):15-20.
31. Iwakiri D, Zhou L, Samanta M, et al. Epstein-Barr virus (EBV)-encoded small RNA is released from EBV-infected cells and activates signaling from Toll-like receptor 3. *J Exp Med.* 2009;206(10): 2091-2099.
32. Iatropoulos MJ, Williams GM. Proliferation markers. *Exp Toxicol Pathol.* 1996;48(2-3):175-181.
33. Hislop AD, Taylor GS, Sauce D, Rickinson AB. Cellular responses to viral infection in humans: lessons from Epstein-Barr virus. *Annu Rev Immunol.* 2007;25:587-617.
34. Rickinson AB, Moss DJ. Human cytotoxic T lymphocyte responses to Epstein-Barr virus infection. *Annu Rev Immunol.* 1997;15:405-431.
35. Kimura H. Pathogenesis of chronic active Epstein-Barr virus infection: is this an infectious disease, lymphoproliferative disorder, or immunodeficiency? *Rev Med Virol.* 2006;16(4):251-261.
36. Epstein MA, Hunt RD, Rabin H. Pilot experiments with EB virus in owl monkeys (Aotus trivirgatus). I Reticuloproliferative disease in an inoculated animal. *Int J Cancer.* 1973;12(2):309-318.

37. Epstein MA, Rabin H, Ball G, Rickinson AB, Jarvis J, Melendez LV. Pilot experiments with EB virus in owl monkeys (Aotus trivirgatus). II. EB virus in a cell line from an animal with reticuloproliferative disease. *Int J Cancer.* 1973;12(2):319-332.

38. Mosier DE. Immunodeficient mice xenografted with human lymphoid cells: new models for in vivo studies of human immunobiology and infectious diseases. *J Clin Immunol.* 1990;10(4):185-191.

39. Shope T, Dechairo D, Miller G. Malignant lymphoma in cottontop marmosets after inoculation with Epstein-Barr virus. *Proc Natl Acad Sci U S A.* 1973;70(9):2487-2491.

40. Takashima K, Ohashi M, Kitamura Y, et al. A new animal model for primary and persistent Epstein-Barr virus infection: human EBV-infected rabbit characteristics determined using sequential imaging and pathological analysis. *J Med Virol.* 2008; 80(3):455-466.

41. Wedderburn N, Edwards JM, Desgranges C, Fontaine C, Cohen B, de Thé G. Infectious mononucleosis-like response in common marmosets infected with Epstein-Barr virus. *J Infect Dis.* 1984; 150(6):878-882.

42. van Lier RA, ten Berge IJ, Gamadia LE. Human CD8+ T-cell differentiation in response to viruses. *Nat Rev Immunol.* 2003;3(12):931-939.

43. Lim WH, Kireta S, Russ GR, Coates PT. Human plasmacytoid dendritic cells regulate immune responses to Epstein-Barr virus (EBV) infection and delay EBV-related mortality in humanized NOD-SCID mice. *Blood.* 2007;109(3):1043-1050.

44. Schmidt KN, Leung B, Kwong M, et al. APC-independent activation of NK cells by the Toll-like receptor 3 agonist double-stranded RNA. *J Immunol.* 2004;172(1):138-143.

45. Tabiasco J, Devevre E, Rufer N, et al. Human effector CD8+ T lymphocytes express TLR3 as a functional coreceptor. *J Immunol.* 2006;177(12): 8708-8713.

46. Moriya K, Fujie H, Shintani Y, et al. The core protein of hepatitis C virus induces hepatocellular carcinoma in transgenic mice. *Nat Med.* 1998;4(9):1065-1067.

47. Watanabe S, Terashima K, Ohta S, et al. Hematopoietic stem cell-engrafted NOD/SCID/IL2Rgammanull mice develop human lymphoid systems and induce long-lasting HIV-1 infection with specific humoral immune responses. *Blood.* 2007;109(1):212-218.